Results in Engineering 21 (2024) 101802

Contents lists available at ScienceDirect

Results in Engineering

journal homepage: www.sciencedirect.com/journal/results-in-engineering

Investigation of the displacement-based seismic performance of geogrid earth-retaining walls using three-dimensional finite element modeling

Muhammad Akbar [a], Pan Huali [a,*], Ou Guoqiang [a], Muhammad Usman Arshid [b], Bilal Ahmad [c], Tariq Umar [d]

[a] Institute of Mountain Hazards and Environment, Chinese Academy of Sciences, Chengdu 610000, China
[b] University of Engineering & Technology Taxila, Pakistan
[c] Department of Structural Engineering, Faculty of Civil Engineering, Doctoral School, Akademicka 2, Silesian University of Technology, Akademicka Street 5, 44-100, Gliwice, Poland
[d] Architecture and the Built Environment, University of the West of England, Bristol, BS16 1QY, UK

ARTICLE INFO

Keywords:
Seismic analysis
Geogrid earth-retaining (GER)
Conventional gravity-type retaining walls
Finite element modeling
Hollow prefabricated concrete structures

ABSTRACT

This study evaluates the earthquake-induced movement of geogrid earth-retaining (GER) walls. A thorough investigation was conducted on a GER wall model, utilizing a comprehensive finite element (FE) analysis. This research focuses on investigating and designing hollow prefabricated concrete panels and conventional gravity-type stone masonry GER walls. It also displays comparative studies such as the displacement of the wall, deflection of the wall, lateral pressure of the wall, settlement of the backfill reinforcement, vertical pressure of the backfill, lateral pressure of the backfill, vertical settlement of the foundation, and settlements of soil layers across the height and acceleration of the walls of the GER walls. The FE simulations used a three-dimensional (3D) nonlinear dynamic FE model of full-scale GER walls. The seismic performance of models has also been examined in terms of wall height. It was found that the seismic motion significantly impacts the height of the GER walls. In addition, the validity of the proposed study model was assessed by comparing it to the conventional reinforcement concrete and gravity-type GRE wall and ASSHTO guidelines using finite element (FE) simulation results. Based on the findings, the hollow prefabricated concrete panels were the most practical alternative due to their lower deflection and displacement. Based on the observation, it was also found that the hollow prefabricated GER wall is the most viable option, as the settlement and lateral pressure in the former type are high.

1. Introduction

The seismic response of geogrid earth-retaining (GER) walls must be considered due to its direct impact on the stability and safety of structures in earthquake-prone areas [1]. A well-known (GER) construction method uses discontinuous gradual concrete facing panels, and geogrid or steel mesh is the most common backfill soil-reinforcement component [2,3]. This study aims to develop a design for a gravity earth retaining (GER) wall using granular backfill, geogrid reinforcing soil, and hollow precast concrete panels. Numerous researchers have studied the behavior of GER walls in previous earthquakes [4]. The earthquake that occurred in Pakistan in 2005, with a maximum recorded peak ground acceleration (PGA) of 0.6 g, resulted in substantial damage to earth-retaining buildings, bridges, and roads near the epicenter. Additionally, it caused extensive sliding and deformation of conventional earth-retaining walls. The earth-retaining wall underwent substantial displacement and rotation due to the 2019 attack earthquake, which recorded a maximum peak ground acceleration of 0.4g [5,6].

Nonlinear dynamics approaches and empirical adjustments are often used to design the seismic performance and internal stability of (GER) walls. These techniques include well-established concepts of seismic pressure on structures [7,8]. Usually, the lateral pressure of walls, reinforcement settlements, deflection, and displacement are assessed by conducting shaking table tests and finite element simulations for different types of retaining walls [9,10]. The use of the three-dimensional technique (3D FE) in modeling has attracted much

* Corresponding author.
E-mail addresses: akbarmohammad0092@gmail.com (M. Akbar), hlpan@imde.ac.cn (P. Huali), ougq@imde.ac.cn (O. Guoqiang), usman.arshid@uettaxila.edu.pk (M.U. Arshid), Bilal.Ahmed@polsl.pl (B. Ahmad), tariq.umar@uwe.ac.uk (T. Umar).

https://doi.org/10.1016/j.rineng.2024.101802
Received 28 August 2023; Received in revised form 12 January 2024; Accepted 13 January 2024
Available online 22 January 2024

interest in accurately representing GER walls' intricate behavior when subjected to seismic forces [11,12]. Numerous researcher have utilized nonlinear dynamics methods of 3D FE modeling to investigate the seismic response of various retaining walls, providing valuable insights into their dynamic behavior and failure mechanisms [13]. These factors include horizontal strain, settlement of reinforcements, displacement, and overturning, which collectively contribute to the stability and safety of earth-retaining walls in high seismic-risk areas [14]. They consider the nonlinearity of soil-structure interaction and the behavior of the retaining wall system, surpassing the limitations of linear assumptions and response theories, and offer valuable insights into the intricate mechanisms and phenomena during seismic events [15].

In addition to calibrating the resistance factors for the reliability-based methods, the measurements from the instrumented wall case studies have been utilized extensively to evaluate the precision of displacement-based seismic performance design methods included in the current design guidelines [3,16–18]. According to Mirmoazen et al. (2021), instrumented field walls incorporating geosynthetic reinforcement were scarce. The available measured database becomes even more constrained in the case of instrumented walls featuring significant reinforcement spacing. In order to enhance comprehension of the behavior of GER walls featuring extensive reinforcement spacing and compensate for the absence of physical measurements, one approach is to construct numerical models that are subsequently validated against physical measurements (Mirmoazen, S. M. et al., 2022) By utilizing the computed outcomes derived from the validated numerical models, the restricted repository of instrumented case studies can be expanded to encompass a more extensive spectrum of reinforced soil and reinforcement characteristics, reinforcement spacing, loading circumstances, and configurations [19].

The findings of finite element analysis and experimental testing comparing gravity-type and rigid retaining walls indicate that the gravity-type of base-restrained retaining walls significantly influenced the backfill pressure [20]. An in-depth analytical examination of the seismic performance of gravity-type retaining walls [21] focused on the importance of wall height in relation to earth shackling. The finite element (FE) approach was used to analyze the passive behavior of a concrete retaining wall designed to resist gravity forces. The investigation found that the failure domain size increased when base excitation was applied [22]. Emin Hokelekli [23] shows that finite element (FE) analysis may calibrate a nonlinear distribution of backfill pressure behind a GER retaining wall. Multiple studies have used shaking tables, and finite element analysis (FE analysis) on scaled-down models of retaining walls to better understand the impact of dynamic backfill on the wall and its many modes of failure [24]. It was shown that the backfill soil might substantially influence the seismic performance of GER retaining walls. Accurately determining the amount of movement caused by earthquakes in GER retaining walls is crucial for the present approach of designing structures based on their ability to withstand seismic activity [24]. Munoz H. et al. [25] used the Newmark sliding block model to predict the displacement of retaining walls caused by earthquakes. Nimbalkar, Sanjay, and Deepankar Choudhury [26] discovered a non-linear dynamic soil pressure along the height of the basement wall. They also observed that the conventional Mononobe-Okabe (MO) approach provides too cautious estimations of seismic forces when numerically analyzing retaining walls.

In order to examine the seismic characteristics of GER walls, scholars have utilized a blend of sophisticated finite element (FE) simulations and experimental trembling table testing [27,28]. By conducting these experiments, crucial parameters, including forces and displacements, can be measured directly, facilitating a more comprehensive comprehension of the distinct response characteristics displayed by GER walls. Conversely, finite element (FE) simulations replicate the intricate interplay among the soil, wall structure, and backfill material, enabling a more comprehensive examination of stress distribution, internal forces, and displacement patterns within the retaining wall system [29]. Researchers may thoroughly understand the dynamic behavior and failure processes of retaining walls by integrating findings from experimental testing and numerical simulations. This information can then be used to design methods better and improve the seismic performance of retaining walls [30–32]. Although there has been notable advancement in examining the seismic behavior of different kinds of GER walls, there is still a major lack of research in comprehending the displacement characteristics and stability of backfill, particularly in retaining walls [33,34]. The precast reinforced concrete pale walls have become more popular because of their distinctive design and construction methods, which entail few connection points between the face panels and the backfill materials [35,36].

However, these innovative systems' specific behavior and response under seismic loading conditions have not been extensively investigated. This study aims to bridge this research gap by conducting a comprehensive 3D finite element analysis to investigate the seismic response of hollow precast GER walls. The prefabricated wall was eco-friendlier than the traditional GER wall. According to the research, the prefabricated wall outperformed the conventional retaining wall regarding CO2 emissions, greenhouse impact, essential material cost, and embodied energy [37]. The study aimed to establish a technique for conducting a seismic analysis of hollow precast GER wall panels using FE analysis. The use of a 3D finite element analysis attained the achievement. However, seismic performance is the main topic of a rigorous 3D finite element analysis of hollow prefabricated (GER) walls. To the author's best knowledge, there has not been a comprehensive investigation of prefabricated walls for use in highway and infrastructure applications, either experimentally or through FE analysis. As a result, there has been no worldwide discovery of these precast GER wall systems [38].

2. Novelty of the study

This study aims to apply nonlinear dynamic finite element analysis methods to explore the seismic performance of hollow precast reinforced (GER) walls. This will be done in light of the motivations and considerations indicated earlier. This study is the first investigation into the impact of earthquakes on several categories of hollow precast (GER) retaining walls. Using diverse wall model heights may facilitate understanding seismic impacts from development activities across different nations, assisting researchers and policymakers in their analysis and decision-making processes. Parallel to these studies, this research fulfills the research gap by investigating a wide range of factors such as displacement and deflection of the wall, vertical pressure of the wall, horizontal pressure of the wall, lateral pressure of the wall, settlement of the wall, settlement of the mesh; vertical pressure of the backfill; horizontal pressure of the backfill; lateral pressure of the backfill; vertical foundation pressure and settlements of soil layers. (Table 1). Therefore, the researchers assumed the possibility of achieving that goal. These groups can keep their strength regardless of geographic location, although the effect of the factors may vary from country to country. Table 1 demonstrates the factors affecting the seismic performance of GER walls in developing and developed countries.

3. Numerical modeling approach

FE analysis of the three-dimensional models of GER walls to investigate the seismic response [19]. The effects of hollow precast concrete, reinforcement concrete, and conventional gravity-type stone masonry GER walls on the seismic performance of the three different wall heights (5 m, 7 m, 5 m, and 5 m) have been examined and accounted for in parametric studies. The FE analysis results were employed in nonlinear dynamic assessments to understand the models' seismic response better. Consequently, the input base accelerations, also known as accelerograms, have been scaled to be 0.3g times the peak ground acceleration (PGA). The responses of the GER wall, Lateral Pressure of the Wall,

Table 1
Studies determine the factors influencing the geogrid earth-retaining walls (GER) wall under earthquake.

References	Authors (Reference No)	Country	Type of wall-facing	VPW	LPW	SGM	BVP	BHP	BLP	VFS	DDW	AAW	Methodology
[9]	Bourgeois E. 2011	United Kingdom	GER	×	×	×	×	×	×	×	×	×	Numerical simulation
[39]	Zhang, W et al., 2022	China	GER	×	×	×	×	×	×	×	×	×	Numerical analysis Physical test
[32]	Yoo C et al., 2019	Canada	GER	×	×	×	×	×	×	×	×	×	Physical test
[40]	M. Ahmadabadi 2009	Spain	GER	✓	×	✓	✓	✓	✓	✓	✓	✓	Numerical analysis
[36]	Tiwary, A, K et al., 2022	Australia	GER	×	×	×	×	×	×	×	×	×	Numerical simulation, Physical test
[34]	Yu Y. et al., 2015	China	GER	×	×	×	×	×	×	×	×	×	Physical test
	This research	Pakistan	GER	✓	✓	✓	✓	✓	✓	✓	✓	✓	FEA of a different model with model heights

Dynamics analysis of earth-retaining walls (DA) GER, Vertical Pressure of the wall (VPW), Lateral pressure of the wall (LPW), Settlement of Geogrid Mesh (SGM), Backfill Vertical Pressure (BVP), Backfill Horizontal Pressure (BHP), Backfill Lateral Pressure (BLP), Vertical Foundation Settlement (VFS). Acceleration of the wall (AAW), Displacement and deflection of the wall (DDW).

Settlement of the backfill reinforcement, lateral pressure of backfill, deflection of the wall, acceleration of the wall, displacement of the wall, vertical settlement of the foundation, and settlements of soil layers have all been analyzed based on the finite element analysis results. The FE model's boundary conditions were replicated using Abaqus' acceleration and displacement-controlled boundary features [41]. The foundation of the FE model is a pinned support, which is restricted along the vertical y-axis but free to move along the horizontal x-axis [20,25]. Geostatic forces have been discovered in both the backfill and base soil domains. The principal purpose of determining the geostatic pressures was to evaluate the correctness of the FE results and determine whether the forces were in dynamic equilibrium [13].

3.1. Material modelling

As indicated in Table 2, the Abaqus FE model for analysis is built using three classes of materials in this research. The reinforcing geogrid was built using the Abaqus [42] wire element feature, and the walls were made using the concrete-damaged plasticity (CDP) model. Utilizing the Mohr-Coulomb (MC) material model, the constitutive behavior of the backfill was determined. The plane strain conditions have been hypothesized to have contributed to creating the 3D model [41]. Additionally, gravitational forces have been included across the entirety of the FE model. The seismic loading was applied to the foundation of the FE model by using the acceleration along the x-axis. Large-deformation numerical analysis sees the widespread application of the nonlinear dynamic explicit solution approach implemented by the FE program Abaqus [41]. Explicit central difference integration rule and many short-time steps are used in Abaqus' dynamic explicit analyses to address boundary value concerns. The FE analysis results were taken at a low sample rate to reduce noise in the data [43].

The study uses three different retaining walls for simulation: two walls, hollow precast concrete panels, and a third convention gravity-type masonry (GER) retaining wall. Three different GER walls were simulated in the study: one gravity-type, two hollow precast, one reinforcement concrete panel, and a GER wall made of reinforced concrete. Details of the geometry specification are shown in Figs. 1–3. Fig. 1 shows the elements of the hollow precast concrete wall. The numerical model shows an idealised repeating unit made up of panels that are 1 m tall and 1 m wide that span the length of the wall. The usual specifications for hollow precast concrete GER walls are 150 mm wide by 14 mm thick, with the steel reinforcing rebar positioned at a vertical spacing of 250 mm rebar stripe. The numerical model depicts a wall measuring 5 m in height and comprising six modules stretching along its length. L = 4 m represents the length of the reinforced zone, which is equivalent to 1 m H for the wall height H. The L/H ratio of 1 is generally regarded as the optimal value for design purposes [3]. No surcharge loading was applied to the model's upper boundary in the numerical simulations. Table 2 lists the rebar specifications utilized in this investigation. The gravity-type and reinforced concrete rigid ER wall running length is 6 m, and height is 5 m, as shown in Figs. 2 and 3.

Table 2
Geogrid earth-retaining walls (GER) design considerations [32,37].

Parameters	precast retaining wall (SM-W1, SM-W2)	conventional reinforcement concrete wall (CR-W)	Conventional gravity-type stone masonry wall (GM-W)
	Value 5 m and 7 m	Value 5 m	Value 5 m
Wall height	5 m and 7 m		5 m
Backfill soil density	18 kN/m2	18 kN/m2	18 kN/m2
Angle of surcharge	0°	0°	0°
Angle of repose	30°	30°	30°
Density of concrete	30 kN/m^3	30 kN/m^3	–
Density of stone	–	–	23–29 kN/m^3
The safe carrying capacity of soil	150 kN/m^2	150 kN/m^2	150 kN/m^2
Friction angle	40°	40°	40°
Compressive Strength of Concrete	30 N/mm^2	30 N/mm^2	30 N/mm^2
Steel's yield Strength	415 N/mm^2	415 N/mm^2	415 N/mm^2
Factor of safety	1.5 to 2.0	1.5 to 2.0	1.5 to 2.0
Effective cover	40 mm	45 mm	45 mm
Elastic modulus (MPa)	32,000	32,000	32,000
The ratio of Poisson's distribution	0.2	0.2	0.2
Model		Concrete Damage Plasticity model (CDP)	

3.2. Constitutive modeling of the backfill and base case

The role of backfill in the seismic performance of GER walls must be determined by comprehensive parametric laboratory testing of various granular backfill types [9]. For the parametric FE analysis studies, the sand, silt [11], mud [12], rock particles, and silt, send granular soil particles (the current research field investigation) have been taken into consideration as granular backfill materials as shown in Fig. 4. The

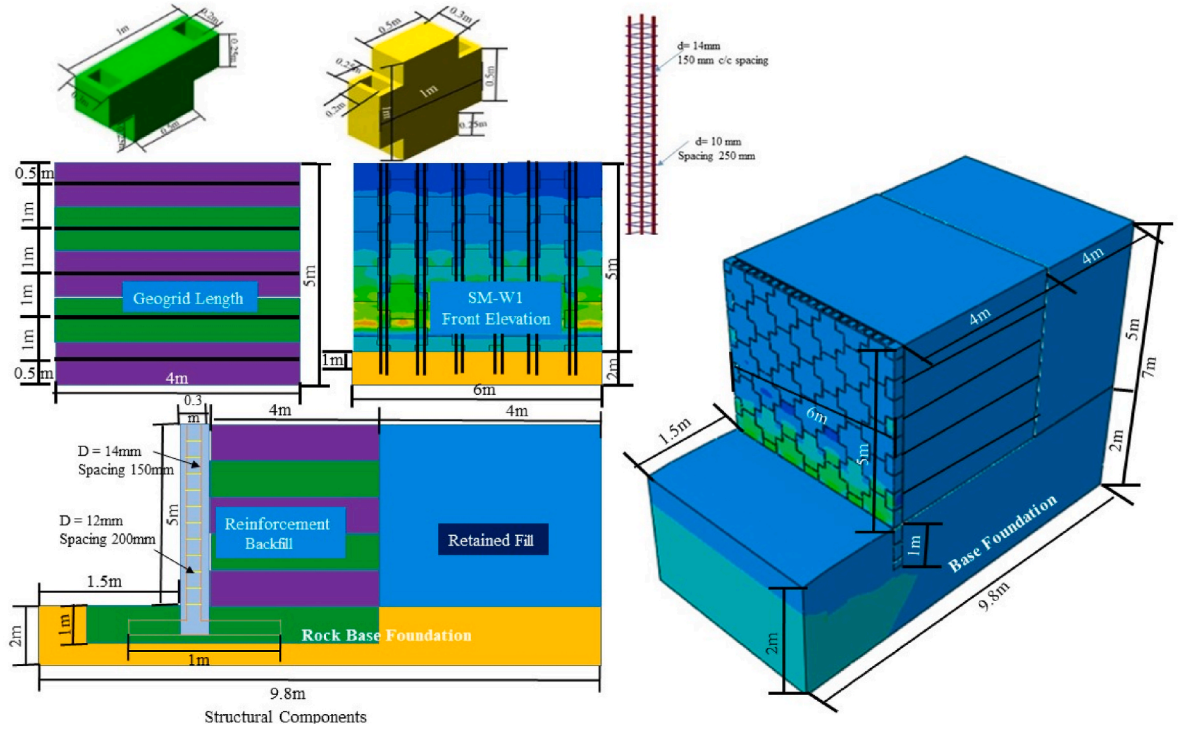

Fig. 1. Overview of 3D model precast hollow concrete structural components of GER wall.

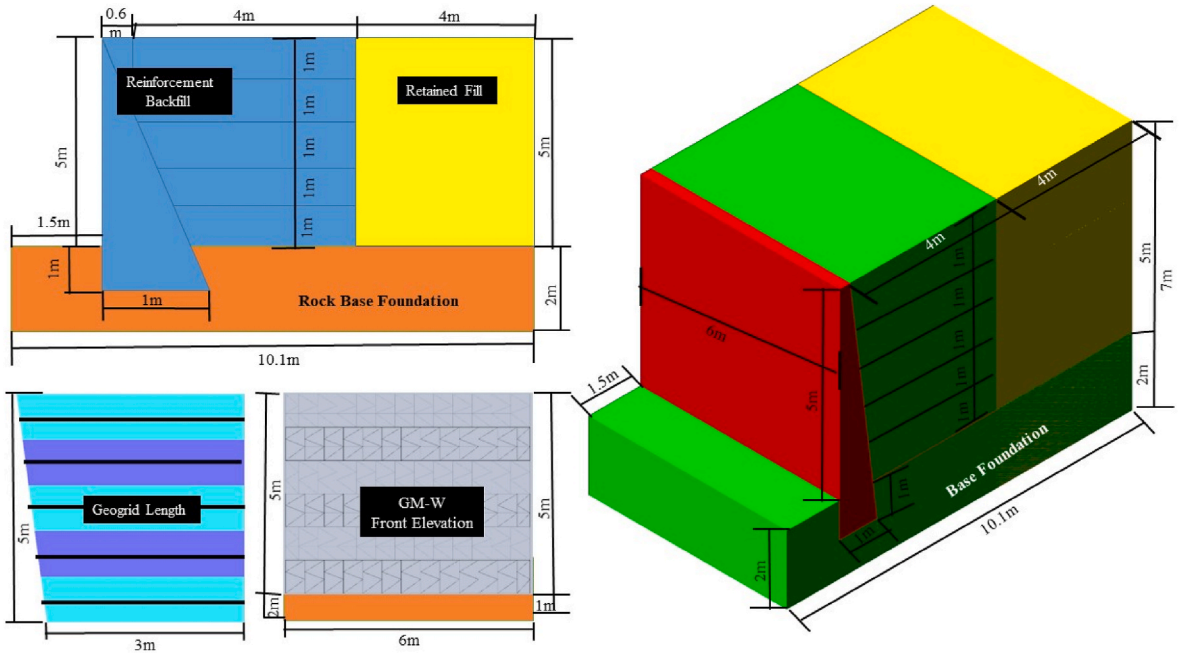

Fig. 2. Complete overview of conventional gravity-type stone masonry wall.

Mohr-Coulomb material model has been utilized to simulate the backfill's constitutive behavior. Several studies [2,43] simulated backfill behavior before and after yield using the MC material model, as shown in Table 3. According to MC, the material model allows for modeling soil behavior after yield [42,44]. This study modeled the geogrid mesh used for backfill reinforcing with weir components in Abaqus, as shown in Fig. 5. Thin reinforcing weirs are layered into the soil for structural support, and weir components mimic their behavior [M. Ahmadabadi, (44)]. It is possible to determine a limit for the reinforcing weir components' tensile failure strain, and these components can give either under tension or under compression.

On the other hand, the weir will bow when subjected to such pressure. The shear behavior at the reinforcing-soil interface is characterized by a nonlinear shear failure envelope that shifts in shape depending on the confining pressure. The reinforcing weir components' characteristics are shown in Table 4, which provides a summary to replicate the geogrid's primary and secondary reinforcement laid.

The materials used as granular backfill in parametric FE analysis experiments. Allen and Bathurst [2] conducted research suggesting that the reinforcement global stiffness, determined by dividing the wall

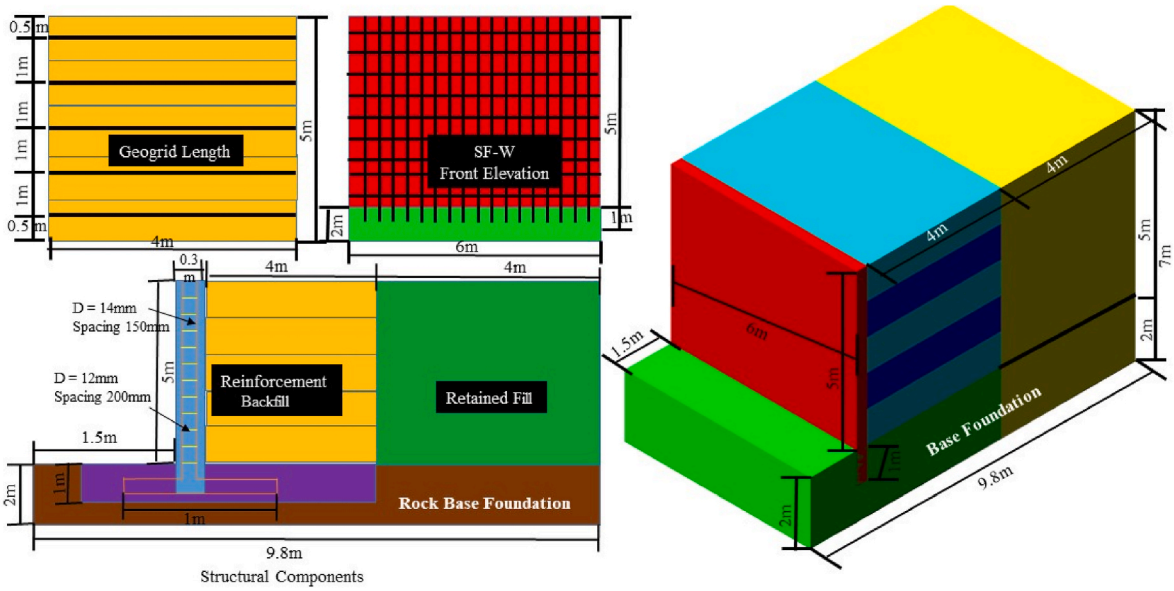

Fig. 3. Complete overview of conventional reinforcement concrete GRE wall.

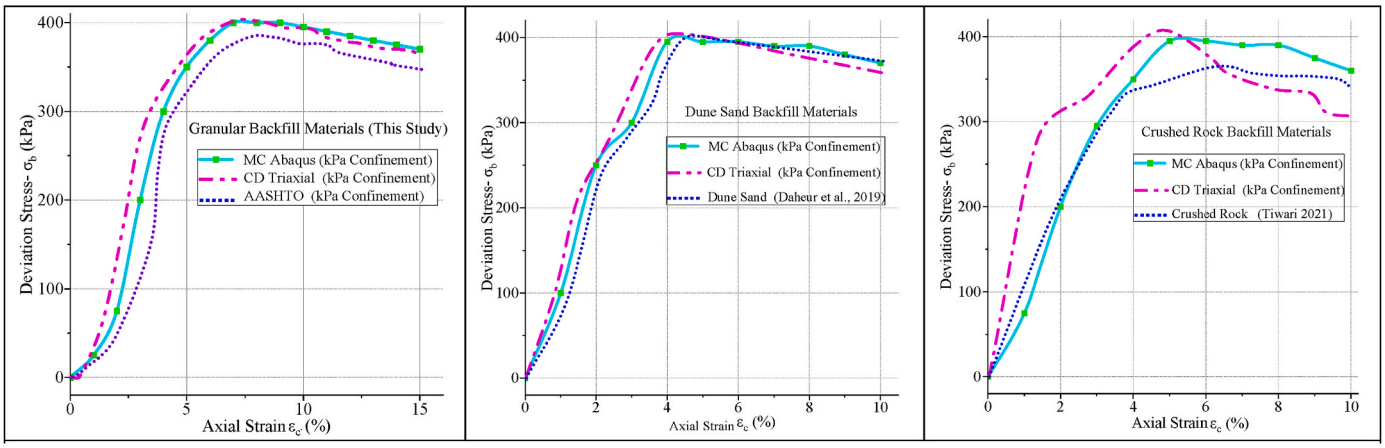

Fig. 4. Constitutive behaviour of different soils considered as backfill.

Table 3
Provides the soil material parameters for the baseline scenario [35].

Parameter	Soil material (Backfill)	Foundation
Unit weight (kN/m^3)	18	20
Elastic modulus (MPa)	20	35
Poisson's ratio	0.2	0.3
Cohesion (kPa)	1	5
Friction angle (degree)	44	36
Dilatancy angle (degree)	14	6
Global stiffness (MPa)	43	43
Reinforcement stiffness J (MN/m)	56	56
Model	Mohr-Coulomb (MC) material model	
Standenrd	AASHT, AFNOR, FHWA	

height (H) by the sum of the stiffness of all reinforcement layers, affects wall performance. For example, an increase in global reinforcement stiffness will result in higher wall reinforcement stresses despite all other parameters remaining constant. According to data from operational full-scale instrumented earth-retaining reinforced soil walls, Allen and Bathurst [7] determined the global rigidity to be between 35 and 380 MPa, with reinforcement stiffness measuring 56 MPa (Table 3). The walls were found to be reinforced with materials that cannot be stretched or extended. The maximum tensile stresses observed in the current study were consistently below 0.03 % for all cases and layers, which is much lower than the yield strain of steel at 0.2 %. On the other hand, Bakr J et al. [8] documented stress levels of up to 0.08 % after building a 17-m-high production (ER) wall under observation. The steel straps in this study experienced maximum strains of approximately 0.2 %, which falls within the lower range of strains observed in real geogrid retaining walls. These values are significantly below the recommended strain of 1 % to maintain the systems at working stress levels [44] and to provide sufficient safety margins against tensile failure [8].

In light of this, the MC model was calibrated in the present investigation using the triaxial test outcomes of all model backfills considered for the FE analysis simulations. Tiwari R [43] produced a comprehensive MC material model that was calibrated using the results of triaxial tests. Different model backfills have been assessed regarding their effects on the calibrated MC material model's outputs regarding triaxial test results (hardening and softening) [35]. The authors [43] detailed the specifics of modeling MC materials, calibrating the post-yield response of backfill using data from triaxial tests, and modeling the Rayleigh damping of backfill.

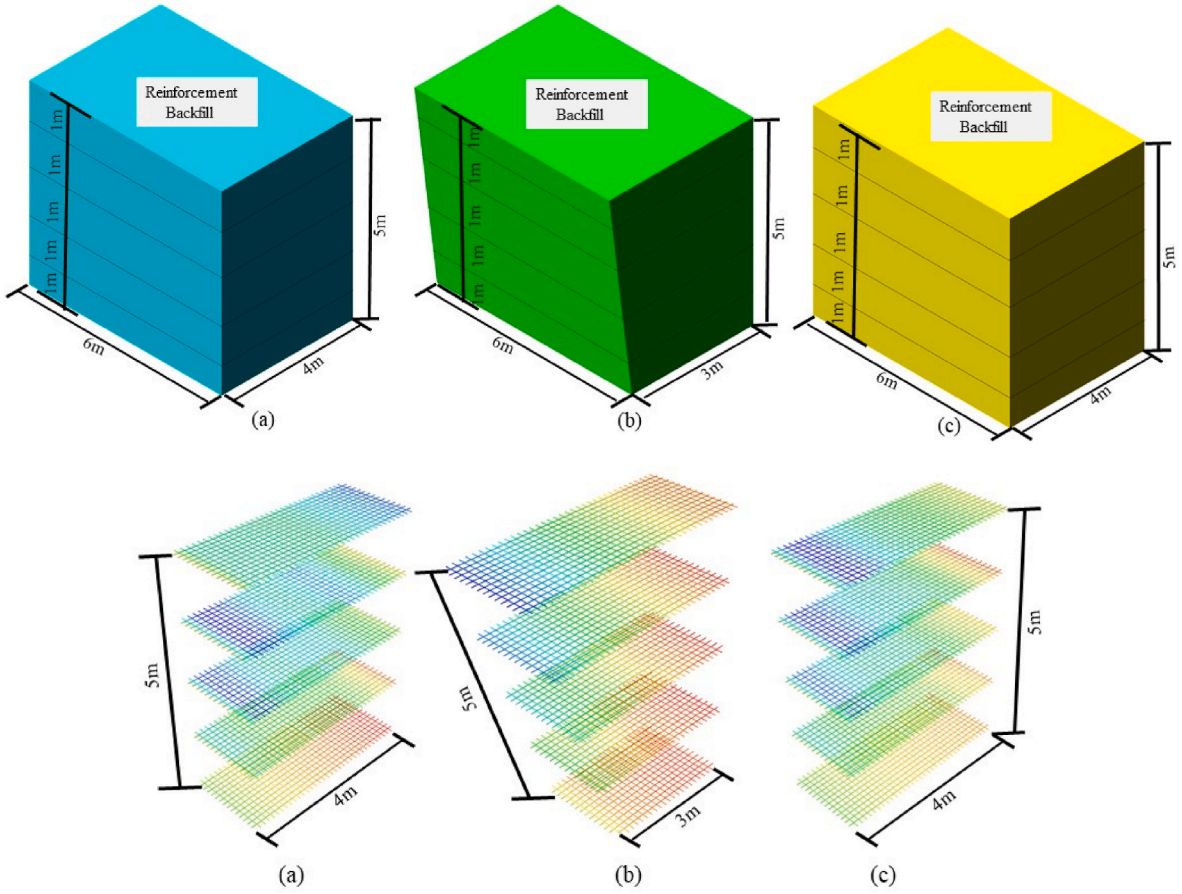

Fig. 5. Modeling of the backfill and backfill reinforcement (a and b) modeling of the precast concrete and gravity-type GER wall backfill (c and d) modeling of the precast concrete and gravity-type GER wall backfill reinforcement.

Table 4
Properties backfill reinforcement material [29].

Parameters	Geogrid
Calculation width (mm)	1000
Number of mesh per calculation width	1000
Mesh thickness (mm)	1000
Elastic modulus (MPa)	2700
Mesh thickness (mm)	3
Tensile stiffness (kN/m)	6400
Tensile stiffness (kN/m)	416
Interface normal and shear stiffness (kN/m/m)	92000
Soil interface cohesion (kN/m)	4.0
Model	Von-Mises plasticity (for Geogrid)
Standenrd	AASHT, AFNOR, FHWA

3.3. Concrete and steel constitutive modeling

The Abaqus FE program was used to simulate the concrete, and the CDP model of concrete-damaged plasticity was used. Numerous researchers have utilized the CDP model to study the constitutive behavior of concrete [25,43]. The CDP model uses the following formulation in Equations (1) and (2) to characterize concrete's constitutive behavior under compression and tension.

$$M_t = (1 - F_t)\, K_0^{vs} : \left(£ - £_t^{vs}\right) \tag{1}$$

$$M_c = (1 - F_c)\, K_0^{vs:}\, \left(£ - £_c^{vs}\right) \tag{2}$$

The tensile and compressive stress vectors are indicated by M_t and M_c, respectively. The $£_t^{vs}$ and $£_c^{vs}$ are the tensile and compressive plastic strain equivalents. The initial undamaged elastic modulus, denoted by the (K_0^{vs}), has been calculated based on the strain and stress response of a uniaxial compressive strength test performed on concrete [45]. Plastic strains are the dependent variables in the damage equation [25]. Lubliner et al. [46] created the first version of the CDP model's yield function, which was later revised by Lee and Fenves [47]. The Abaqus/Explicit User's Manual [41] has information on the CDP yield function. There is no associative flow in the CDP model. The eccentricity and the dilation angle control the plastic potential process, measured at the deviatoric stress plane.

$$B_{f=}\, 1.4 \left(\frac{Sfc\ -8}{10} \right)^{2} /^{3} \tag{3}$$

$$J_g = \left(0.0469 a_g^2\ -\ 0.5 a_g + 26\right) \left(\frac{Sfc}{10}\right)^{0.7} \tag{4}$$

Table 2 displays the material characteristics considered using the CDP model to model concrete. Carreira and Chu [9] proposed a method for generating the stress-strain response of concrete with a characteristic strength (S_{fc}) of 30 MPa. When the stresses in concrete reach a level greater than 0.3 S_{fc}, it was hypothesized that the material would begin to act in-elastically (when subjected to compression). When subjected to uniaxial stress, the fracture energy approach predicted the concrete's tensile behavior [40]. A linear softening model has been used to indicate the tensile failure of concrete. We used Equations (3) and (4) to figure out B_f, which stands for the tensile strength of the concrete, and J_g, which stands for the fracture energy. Both the concrete compressive strength (S_{fc}) and the maximum aggregate size (a_g) have been used in the process of determining the B_f and the J_g, respectively [41,45].

3.4. Load and boundary conditions

The boundary conditions, zone dimensions, and property assignment substantially influence the facing behavior of these wall types, as demonstrated by the numerical modeling; these parameters play an essential role in the model simulations. The base of the model, which is 2 m below the wall, was found to be far enough away that it didn't have any noticeable effect on the results. The finite element mesh was made up of ten nodes for each element. These nodes were used to model the interactions between different materials. The finite element mesh was made up of 14,888 nodes and 13,128 elements. One connection is between the bottom of the foundation soil horizontally and vertically. Two connections are between the retained soil horizontally on both sides. Three connections are horizontal between the retained soil on its left side. The limits of the FE model were set by ABAQUS's acceleration and displacement-controlled boundaries condition. The FE model is built on a pinned support that limits movement along the y-axis but allows movement along the x-axis [8,35]. It has also been found that the backfill and base soil have geostatic loads. The main reason for giving a detailed report of the geostatic stresses was to check that the FE values and force distribution were correct [13]. The x-axis acceleration was used to load the base of the FE model with earthquake forces. The domain lines could move up and down without problems in the front foundation zone and the reserved fill zones. It was a practical solution to find the wall-facing distance from the back boundary of the domain in order to keep the far-field boundaries from having too much of an impact on the GER wall's deformations and length.

The primary purpose of providing a detailed explanation of the geostatic pressures was to confirm the finite element analysis's accuracy and the forces' distribution [42]. The y-z borders in the vertical direction were fixed along the x-axis of the cross-plane. Consequently, the GER wall's vertical (y) limits and panels, y–z, had no restrictions on their movement. The domain borders were positioned vertically at the front of the foundation zone and the back of the retained fill zone. The x-axis acceleration was used to provide seismic loading to the foundation of the FE model. The domain borders showed unhindered vertical movement in both the preserved fill areas and the frontal foundation area. The model's bounds were restricted concerning all degrees of freedom of the system (DOFs) [35]. The spring and dashpot system simulated the finite element model's vertical (viscous) limits. The use of viscous boundaries has been effective in reducing boundary effects and computing time.

3.5. Mesh sensitivity analysis of model

The effects of various mesh sizes on the seismic response of the GER wall have been investigated through mesh sensitivity analysis. The FE model uses planar strain elements with lowered integration and hourglass control (CPE4R), except for the steel reinforcement. We used the beam element (B31) to get the desired mesh for the rebar. Several researchers have examined the link between mesh size and structural response, and their findings have led them to conclude that the results of FE analysis are sensitive to mesh size. Choosing a suitable mesh size makes it possible to acquire correct FE findings with a minimum computing effort [8,20]. Shaking table tests on the simplified FE and retaining wall model analyses by Tiwari and Lam [43] demonstrate that the backfill at the base-restrained retaining wall's stem and heel significantly influences the base-restrained retaining wall's seismic response. The researchers discovered this. Several mesh sizes were used for sensitivity analysis at the contact sites between the GER wall and the backfill. This research used a finite element model to determine how mesh size affects computational results, aiming to use the most accurate and relevant modeling technique possible. The mesh size of the final models is relatively small, with a mesh element size of 25 mm being used for all of them [20].

3.6. Simplified analytical model

FE study on GER wall models estimates earthquake-induced displacement. FE investigations on full-scale GER wall models need FE simulation and constitutive modeling competence. A force-based displacement check model has been proposed to estimate the GER wall's maximal earthquake-induced elastic displacement (£max) with granular backfill. Fig. 6 depicts the GER wall considered during formulation development. The GER wall's height and thickness are denoted by ''h'' and ''w_t''.

Determine the body force at the GER wall's unit height.

$$(\boldsymbol{M1_{CD}})\boldsymbol{W1_{AE}} = \boldsymbol{HF_A\ X\ C_k\ X\ \omega_{wall}} \tag{5}$$

Backfill dynamic pressure coefficient according to the Mononobe-Okabe (MO) model

$$K_{AE} = \frac{cos^2(\varnothing - \theta - \alpha)}{cos\ \varphi\ cos^2\theta\left(\Delta + \theta + \alpha\left[1 + \sqrt{\frac{sin(\Delta+\varnothing)sin\ (\varnothing-\gamma-\alpha)^2}{cos(\Delta+\theta+\alpha)cos(\gamma-\theta)}}\right]\right)} \tag{6}$$

Dynamic soil pressure at the base of the GER wall

$$S_{AE} = HE_A K_{AE} \Delta_{backfill} h \tag{7}$$

Utilize the (S_{AE}) to represent a triangular load per GER wall unit width.

$$(M2_{CD}) \tag{8}$$

Determine the greatest possible movement caused by the inertia of the GER wall.

$$£1_{max} = \left(\frac{B1_{Fs}\ h4}{8EI}\right)\text{GER}\ Wall = (HF_A\ X\ C_k\ X\ \Omega_{\text{wall}}) \tag{9}$$

Calculate the maximum displacement caused by dynamic soil pressure.

$$£1_{max} = \left(\frac{B1_{Fs}\ h4}{30EI}\right) \tag{10}$$

Determine the utmost elastic displacement exhibited by the base retained.

$$£_{\text{max}=}\ £1_{max} - \ £2_{max} \tag{11}$$

Fig. 4 depicts the seismic body force ($M1_{CD}$) on the GER wall stem and the dynamic soil force per unit width of the wall ($M2_{CD}$) along the wall height (assuming a triangular distribution). It supports a homogeneous, horizontal, granular backfill behind it, and it should be highlighted. The backfill contact angle (ø) has been considered to be ø/2. The MO equation has been used to predict the seismic pressure behind the GER wall stem [31]. The pseudo-static pressure on the GER wall stem is calculated using the MO equation, and it grows linearly with wall depth. The pseudo-static lateral pressure coefficient (S_{AE}) was calculated to be 100 % S_h. Eq. (6) calculates the seismic force (S_{EA}) along the GER wall height.

Where AF_H is the backfill's horizontal acceleration amplification. The formulation utilized to determine the maximum displacement resulting from the wall inertia forces ($£1_{max}$) has been computed as follows: The variables used in this context are E, representing Young's modulus of the GER wall; I, representing the moment of inertia of the facing panels; backfill, representing the unit weight of the backfill, k_h, representing the horizontal seismic coefficient, and W_{wall}, representing the weight of the model. The calculation of ($£2_{max}$), which represents the maximum displacement resulting from seismic active pressure of backfill, has been determined utilizing the subsequent formulation: The equation $(M2_{CD}) = S_{AE}$ Indicates the seismic force per unit of GER wall breadth. After computing $£1_{\text{max}}$ and $£2_{\text{max}}$, these values can be used to determine the utmost displacement at the model's apex. The process for estimating the earthquake-induced elastic displacement of the GER wall

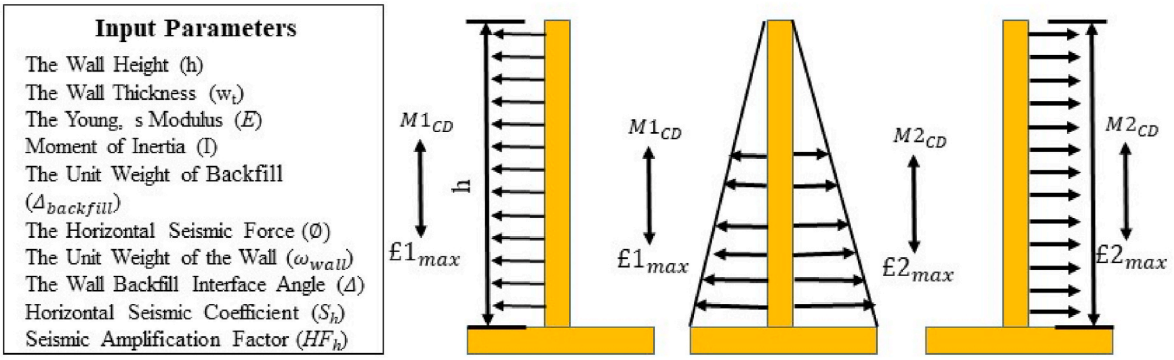

Fig. 6. Input estimating GER retaining wall maximum elastic seismic displacement.

with granular backfill is illustrated in detail in equations (5)–(11).

3.7. Validation of FE modeling approach

In this work, the authors conducted conventional gravity-type, reinforcement concrete, and hollow precast concrete wall panel GER walls model results to validate the capabilities of the current FE modeling technique. A 3D plane strain FE analysis model of the full-scale wall model has been created using the FE modeling method. The backfill was modeled using the MC material model, and all wall models were modeled using the elastic material characteristics. Analyses of nonlinear time histories have been carried out with the help of the dynamic explicit scheme that the FE program Abaqus provides. It is important to note that the recorded displacement time history of the historical

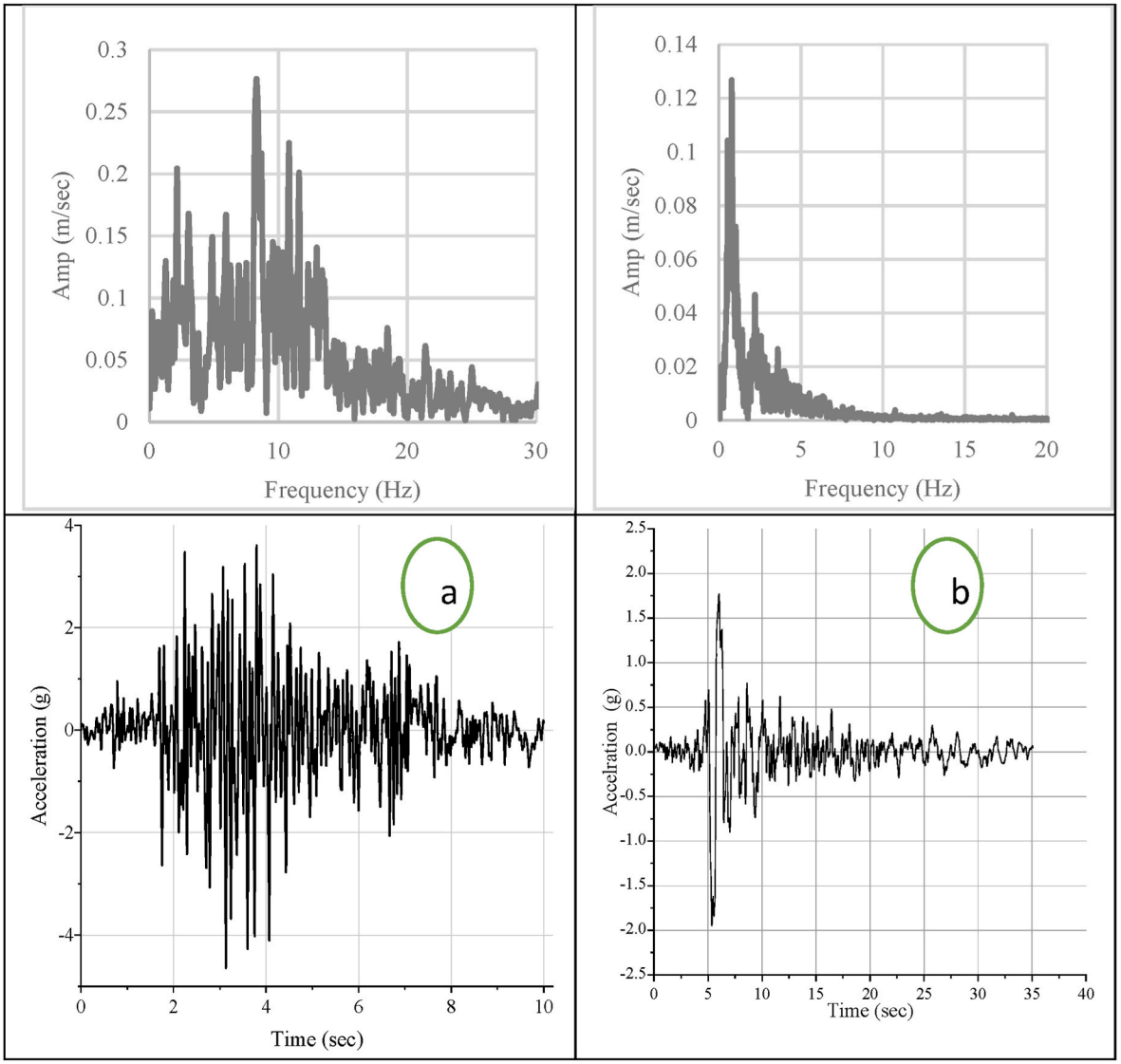

Fig. 7. Seismic input motion.

earthquake shaking wave was utilized to construct the input base excitation for the FE models. Simulation results correlate very well with those from the all-walls model. The seismic force of the prototype base retained retaining walls connects instead well [43]. This indicates the current FE modeling technique can reproduce the seismic response of GER walls in a virtual environment in an accurate manner.

4. Seismic input excitations

This research explores the seismic behavior of GER walls using an FE analysis under earthquake conditions equivalent to those utilized in the analysis's base movements. Harmonic excitations of changing amplitudes and frequency were used as the basis for the model's initial movements. The strength of these stimulations was gradually raised from low peak acceleration amplitudes for brief periods to high peak acceleration amplitudes for a specific time. It is depicted that the time history of the wave acceleration was applied to the model for evaluation. Fig. 7 (a and b). shows how to produce this wave motion by extrapolating data from the area where the latest earthquake occurred [5,6].

4.1. Model approach applied to case study

The baseline model parameters were sourced from the study conducted by Yu et al. (38), which focused on modeling the instrumented reinforcement wall at the Public Works Department (PWD) in Pakistan, as documented by Ref. [6]. To establish a higher confidence level in the 3D model created for this investigation, the authors and their colleagues reexamined the deflection and lateral pressure toe load observed and numerically predicted in a previous study [49]. The material characteristics used for the numerical analysis of the (GER) wall have been determined in the previously provided tables. It is essential to acknowledge that the GER wall was a prototype to maintain a rather slender embankment subjected to an angled surcharge. The wall was built using cruciform-shaped facing panels. Therefore, the overall configuration was more intricate than the three-dimensional wall segment, the primary subject of investigation in the present work.

The situation of conventional concrete and Gravity-type retaining walls after an earthquake is depicted in Fig. 8 (a, b). The 3D numerical and measured results reasonably agree with the physical system's complexity. In this study using the 3D FE model, it was determined that increasing the structural elastic modulus from its initial value improved the overall accord between measured and predicted values. Yu et al. [35] reported the 2D numerical model results using the program FLAC 2D, and the authors performed the 3D modeling using the program ABAQUS. When comparisons are limited to reinforcement stresses, it is possible to conclude that the 3D model has no practical advantage over the 2D models. The disadvantage of the 2D approach is that discontinuous reinforcement loads must be regarded as continuous elements along the plane of strain (x). This challenges GER walls with variable horizontal spacing between reinforcement backfill layers, such as the Minnow Creek wall in the United States, as studied by Ref. [32].

5. Results & discussion

The results obtained from analyzing various parameters related to hollow precast walls (SM-W1 and SM-W2) and traditional retaining walls (CR-W and GM-W) under seismic loading conditions are discussed in this section. The results include vertical pressure, horizontal pressure, lateral pressure, settlement of the backfill, backfill vertical pressure, backfill horizontal pressure, backfill lateral pressure, Vertical Settlement of the Foundation, deflection of the wall, displacement of the wall, acceleration of the wall in vertical and horizontal directions. The analysis provides valuable insights by comparing our results with those of previous researchers; we gain valuable insights into the behavior and performance of these different wall types, allowing overall effectiveness in mitigating the effects of seismic events.

5.1. Lateral pressure of the wall

Fig. 9a is a detailed analysis of the lateral pressure distribution on (SM-W1, SM-W2, CR-W, and GM-W) under seismic loading conditions. The incremental active lateral wall pressures were predominantly positive up to the lower part of the wall. This indicates the transmission and distribution of lateral forces within the walls. When comparing the performance of the different wall types, SM-W1 and CR-W demonstrated better lateral pressure distribution than SM-W2 and GM-W. These findings provide valuable information on the performance and lateral pressure of different types of GRE walls under seismic loading conditions. For instance [Wang, K et al., 2022], conducted a comprehensive study on the lateral pressure distribution of varying wall types under seismic loading. Therefore, the passive deformation earth pressure mainly affects the retaining wall for the passive state. Our analysis aligns with their observations, as SM-W1 and CR-W demonstrated better lateral pressure performance than SM-W2 GM-W. Additionally, [Tiwari R and Lam N (2021)] investigated the behavior of earth-retaining walls under seismic conditions and analyzed their response to lateral pressures. Our results corroborate their findings, as we observed similar patterns in the distribution of lateral pressures along the height of the

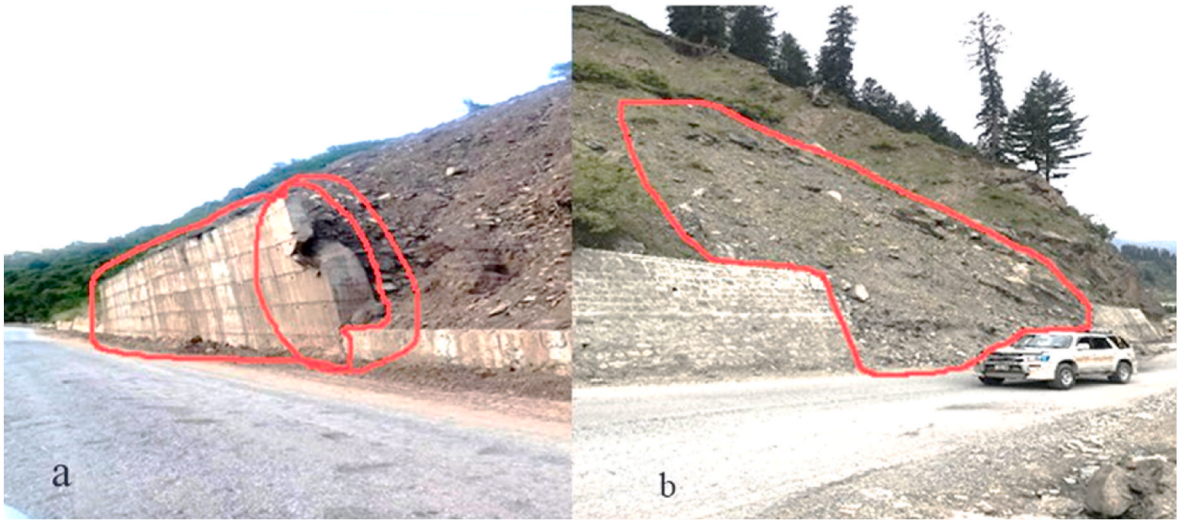

Fig. 8. (a) 3D model overview: (b) precast hollow concert structural components (case study).

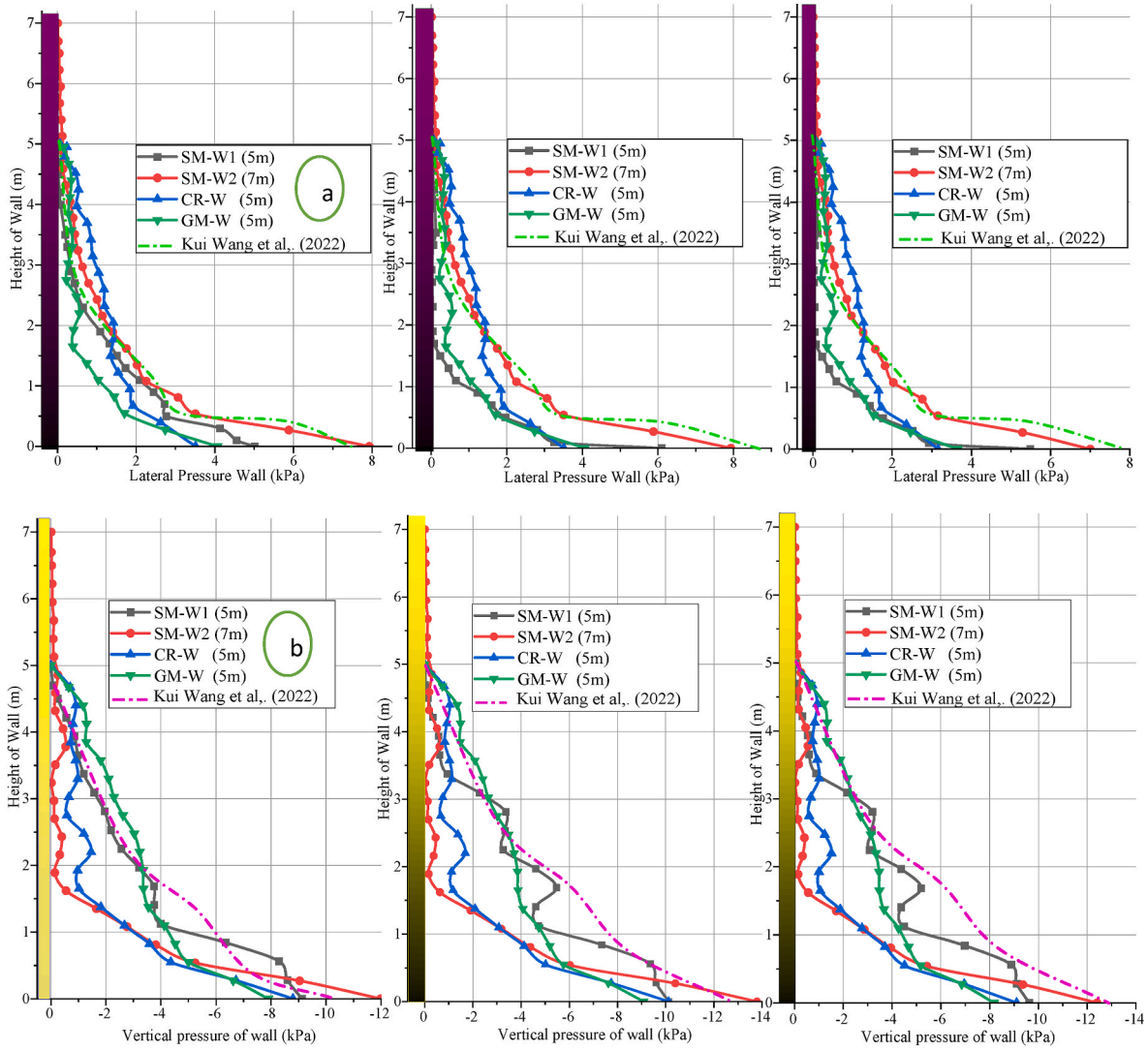

Fig. 9. Lateral pressure of the wall (a) Lateral pressure of wall (b) Vertical pressure of the wall.

walls.

The distribution of walls (SM-W1, SM-W2, and GM-W) under seismic loading conditions. Analysis of vertical pressure reveals significant variations in pressure distribution along the height of the walls. Fig. 9b demonstrates that SM-W1 has unique behaviour with lower negative vertical pressure than SM-W2 and GM-W, indicating superior performance under vertical pressure. These findings are consistent with the results obtained in a previous study by [Ling HI et al., 2005], highlighting the influence of wall height on vertical pressure distribution. Our study further confirms the importance of considering wall height as a crucial factor in designing walls capable of withstanding vertical pressures. To summarize the results of the vertical pressure, Fig. 9b depicts that the SM-W1 exhibits a more favourable response to vertical pressure than SM-W2 and GM-W. Furthermore, comparing our results with previous researchers is crucial to validate our findings and contribute to the existing body of knowledge [Munoz H et al., 2012; A. Athanasopoulos Zekkos et al., 2013]. By examining the literature, we can identify similar trends and patterns in the behavior of different wall types under seismic loading conditions, confirming the reliability of our analysis and gaining a broader perspective [Liu, H. (2012)]. This comparative approach allows us to establish the robustness of our findings and further strengthens the credibility of our study.

5.2. Settlement of the backfill

Fig. 10 inset depicts the backfill reinforcement settlement behind the SM1-W, SM2-W, CR-W, and GER walls. The incremental settlement of the backfill reinforcement of the wall has been observed, and it is found that under the influence of seismic excitation, the backfill reinforcement has a similar time history of settlement trend with the increasing order by SM1-W, SM2-W, CR-W, and GM-W. The phenomenon of gradual settlement of the geogrid positioned at the rear of the backfill has been documented. It has been determined that when the backfill reinforcement is subjected to seismic excitation, the settlement patterns closely resemble the ascending order of settlement observed in the SM1-W, SM2-W, CR-W, and GM-W GER walls. Fig. 10 (a and b) depicts vertical settlement profiles for geogrid-supported backfill reinforcement layers. The datum for these plots is the wall toe elevation at the beginning of the wall construction. The settlements increase with time and distance from the face and are greater for geogrid reinforcement backfill materials that are more extensible.

The maximum settlement of walls (SM1-W, SM2-W, CR-W, and GM-W) is approximately 5 mm and 8 mm, 7 mm and 15 mm, 12 mm and 20 mm, and 37 mm and 42 mm, respectively. The finding demonstrates that for each wall case in each plot, the minimum settlements are close to the connections, which is consistent with the soil drooping over the geogrid reinforcement as previously described. The findings indicate that the

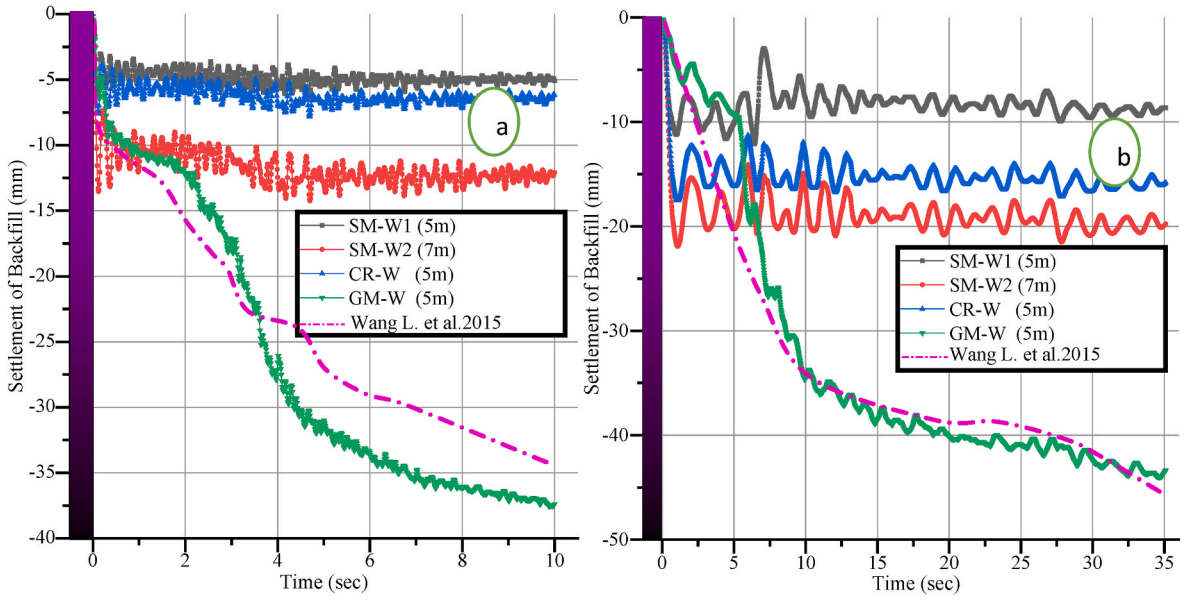

Fig. 10. Settlement of the backfill reinforcement.

SM1-W and CR-W backfill mesh exhibited significant resistance to settling under seismic loading conditions. On the other hand, it was seen that the SM2-W2 and GM-W backfill meshes shook a lot when they were exposed to seismic forces. This showed that the SM-W1 and CR-W reinforcements are more reliable than the SM-W2 and GM-W walls. For instance, [Wang et al. (2015)] studied the settlement behavior of geogrid-reinforced walls under seismic excitation. Their research highlighted the time-dependent settlement patterns and emphasized the importance of considering the long-term effects of seismic excitation on geogrid-reinforced walls.

5.3. Lateral pressure of backfill

A detailed analysis of the lateral pressure distribution in the backfill of (SM-W1, SM-W2, CR-W, and GM-W) walls under seismic loading conditions. The analysis of lateral pressure distribution along the height of the walls revealed distinct patterns. The incremental lateral backfill pressures were predominantly lower around one-third of the wall's height and transitioned to positive values after the mid-level. This observation suggests a shift in the lateral pressure distribution along the height of the walls. SM-W1 and CR-W exhibited similar performance in terms of lateral pressure. Fig. 11a demonstrated that these walls were subjected to primarily lower lateral pressures at one-third of their height, suggesting their capacity to endure and resist lateral forces. On the contrary, SM-W2 and GM-W exhibited high lateral pressure. This alternating pattern suggests potential instability and oscillation in the lateral response of SM-W2. In summary, the backfill lateral pressure distribution analysis highlights the distinct patterns observed along the height of the walls. SM-W1 and CR-W exhibit similar performance with predominantly lateral pressures, indicating their stability and resistance to lateral forces. SM-W2 shows alternating high lateral pressures, suggesting potential instability.

We can validate and contextualize our results by comparing our findings with those of previous researchers. This comparison allows us to gain insights into the behavior of backfill lateral pressure and its impact on the stability and seismic performance of backfill. The findings of previous studies [Munoz H et al., 2012, Wang K et al., 2022] support the stability exhibited by SM-W1 and GM-W under lateral pressure. The ability of SM-W1 and GM-W to withstand and resist lateral forces, as indicated by predominantly negative lateral pressures, is crucial for the stability and performance of retaining walls. These walls demonstrate their capacity to effectively distribute and resist lateral forces exerted on them. On the contrary, the alternating positive and negative lateral pressures observed in SM-W2 and CR-W suggest potential instability and highlight the need for further investigation into its lateral response. The findings emphasize the advantages of SM-W1 and GM-W in terms of lower lateral pressure.

A comprehensive analysis of the vertical backfill pressure of the SM-W1, SM-W2. CR-W and GM-W walls under seismic loading conditions. The analysis of backfill vertical pressure revealed that the pressure decreased with depth below the foundation. As the depth below the foundation increased, the vertical earth pressure exerted on the backfill decreased. This observation suggests that the depth below the foundation significantly influences vertical pressure distribution in the backfill. Furthermore, the findings indicated that backfill height also influences the foundation pressure. A higher vertical ground pressure on the backfill resulted from a higher wall height. Fig. 11b illustrates and accentuates the benefits of SM-W1 and GM-W in terms of decreased vertical pressure. On the contrary, the alternating high negative vertical pressure observed in SM-W2 suggests potential instability in its vertical pressure response. For instance [Wang et al., 2015], conducted a comprehensive study on the vertical pressure behavior of GER walls under seismic excitation. Our analysis supports the findings of [Munoz H et al., 2012, Wang K et al., 2022], as we also observed the impact of seismic excitation on the vertical pressure response of the walls and emphasized the importance of considering seismic forces in the design and construction of GER walls.

A comprehensive analysis of the backfill horizontal pressure exerted on the SM-W1, SM-W2, and CS-W walls under seismic loading conditions. The results indicated that these pressures were predominantly negative, particularly in the lower section of the walls. This observation suggests that the backfill stabilizes the walls, resisting the horizontal forces applied to them. Fig. 11c SM-W1 and GM-W demonstrated stability under horizontal pressure, similarly resisting horizontal pressure forces. In contrast, SM-W2 experienced more significant horizontal tensions. The analysis showed that SM-W1 and GM-W exhibited better resistance to horizontal pressure than SM-W2. In summary, the analysis of backfill horizontal pressure highlights the stabilizing effect of the backfill on the walls and the differences in the performance of various wall types. The observations made by [Munoz H et al., 2012, Wang K et al., 2022] regarding the stabilizing impact of backfill align with our findings, confirming the role of backfill in mitigating horizontal

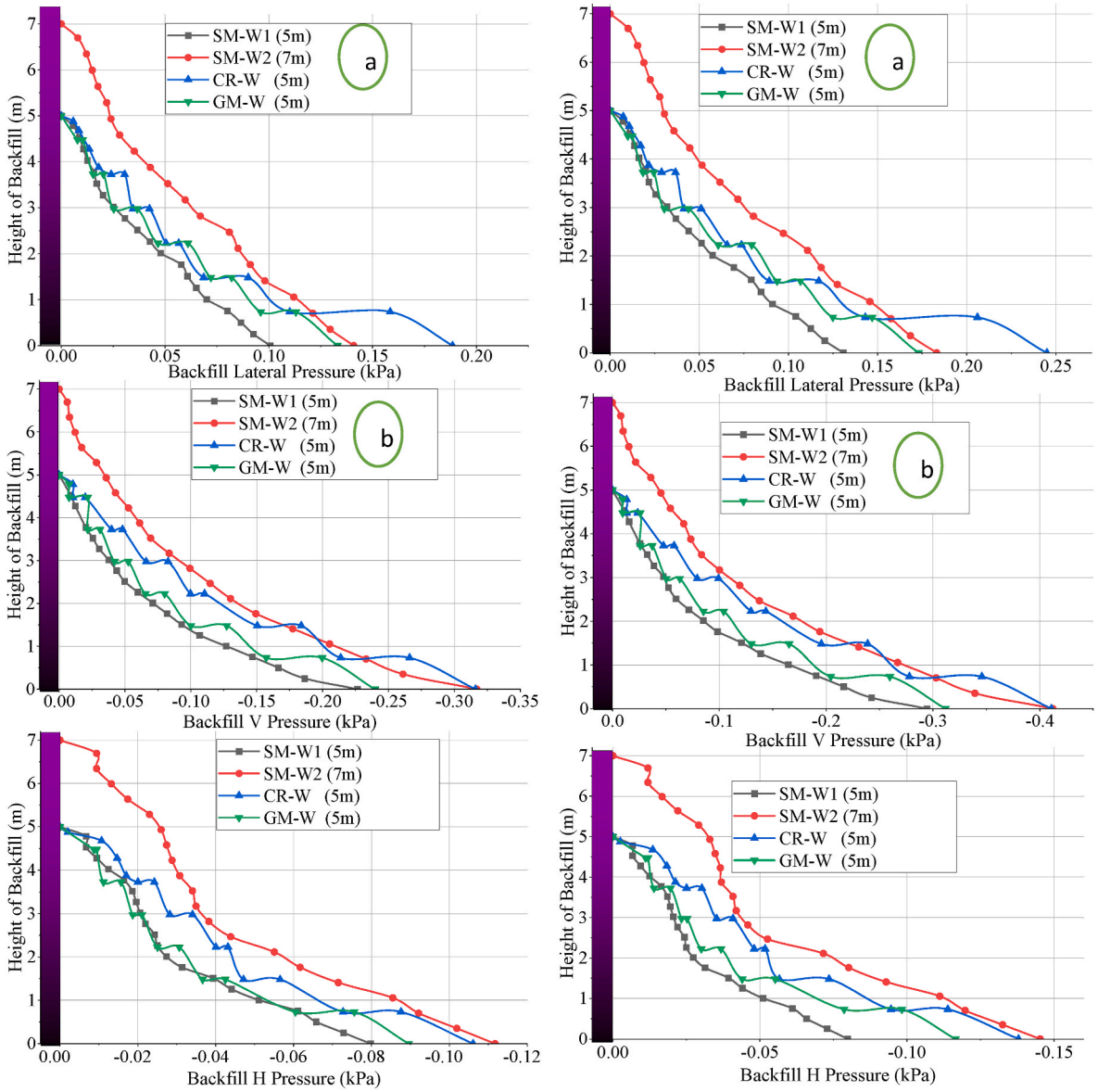

Fig. 11. Lateral pressure of backfill (a) Lateral pressure of wall (b) Vertical pressure of wall (c) Horizontal pressure of the wall.

pressures and examining the similarities and differences in the response of different wall types to horizontal pressure. This comparative approach allows us to establish the reliability of our analysis and provides a broader understanding of the behavior of backfill horizontal pressure in GER wall design.

5.4. Deflection of the wall

The distribution of earth pressure on the wall is very different under rotation around the wall, the base point, and the top, and the influence of the soil constraint at the bottom of the wall cannot be ignored when solving the ultimate pressure on the earth. The deflection on a vertical line along the wall's height. It is evident from the retaining wall's height increase, deflection decrease, and it becomes highest at the bottom. Fig. 12 displayed the reflection diagram, which exhibited the reverse patterns compared to the stress diagrams. The amount of deflection in the SM-W1, SM-W2, CR-W, and GM-W GRE walls grew from lowest to highest as the wall rose in height. It indicates that the upper area of the wall experiences the highest deformation. Similar deflection behavior was observed in CR-W walls, as depicted in Fig. 12 (a and b). However, the deflection behavior in the SM-W1 differed from that of the other walls models. The continuous deflection in the SM-W2 and GM-W retaining wall after 1.5 m of wall height progressively increases deflection with the wall's height.

To validate the consistency of our results and contribute to the existing body of knowledge, we compared our findings with those of previous researchers who have investigated deflection behavior in retaining walls under seismic loading conditions. For instance [Tiwary A, K et al., 2022], conducted a study on the dynamic response of retaining walls, including deflection analysis. Their research emphasized the importance of accurate prediction and control of deflection to ensure the stability and performance of retaining walls under seismic forces. Similarly [Tiwary A, K et al., 2022], investigated the behavior of different types of retaining walls under seismic loading, focusing on evaluating deflection behavior characteristics. Their study provided valuable information on the factors that influence the response to deflection and offered design recommendations to improve the performance of the walls. However, the deflection distribution behavior in SM-W1 walls differed from that of SM-W2, CR-W, and GM-W walls. The wall deflection distributions (SM-W1, SM-W2, CR-W, and GM-W) are about

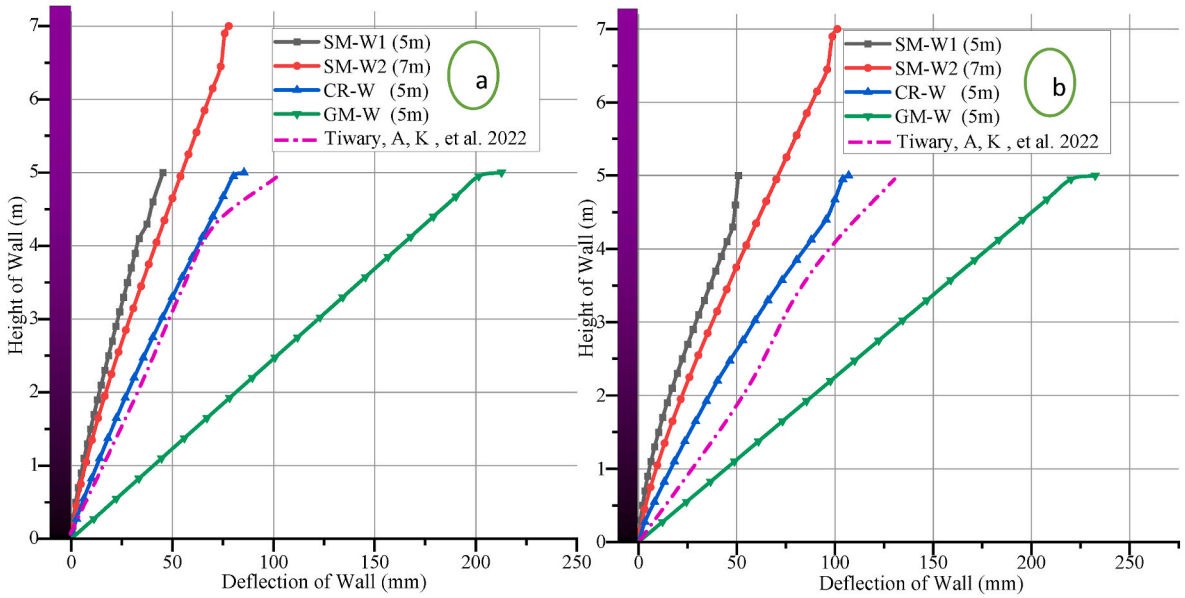

Fig. 12. Deflection of the wall.

44 mm, 89 mm, 200 mm, and 80 mm, respectively.

5.5. Acceleration of the wall

Vertical and horizontal acceleration analysis played a crucial role in assessing the dynamic behavior and stability of the analyzed walls during seismic events. By analyzing these parameters, valuable insights were gained into SM-W1, SM-W2, CR-W, and GM-W response to seismic loading, highlighting their unique acceleration patterns, as shown in Fig. 13. The analysis revealed vertical and horizontal acceleration variations among the different wall types. SM-W1, SM-W2, CR-W, and GM-W exhibited a maximum vertical acceleration of [X] and a maximum horizontal acceleration of [Y]. These findings emphasize the influence of seismic loading on the response of walls and highlight the importance of understanding and considering vertical and horizontal acceleration characteristics to evaluate their stability and ability to withstand seismic forces.

To validate our findings and contribute to the existing knowledge and understanding of GER wall performance under seismic loading, we compared our results with those of previous researchers who have investigated the behavior of vertical and horizontal acceleration in retaining walls. For instance [Munoz H et al., 2012], conducted a study on the dynamic response of retaining walls under seismic forces and analyzed the acceleration characteristics. Their research emphasized the importance of accurately assessing vertical and horizontal acceleration to evaluate the stability and performance of retaining walls. Similarly [Tiwary A. K. et al., 2022], investigated the seismic response of different retaining wall types and examined the acceleration behavior. Their study provided valuable insights into the factors that influence the response to vertical and horizontal acceleration and offered recommendations to improve the seismic performance of retaining walls. In conclusion, the comprehensive vertical and horizontal acceleration analysis provides crucial insights into the dynamic behavior and stability of precast and traditional masonry walls during seismic events. The distinct acceleration patterns observed in SM-W1, SM-W2, CR-W, and GM-W highlight the influence of seismic loading on their response. However, the acceleration behavior of the GER wall in both directions, SM-W1 and CR-W, differed from that of SM-W2 and GM-W walls. Furthermore, our analysis, which further supports the stability and resistance to acceleration behavior of SM-W1, is superior.

5.6. Vertical settlement of the foundation

The research problem is the plane strain problem, and the longitudinal extension of the GER wall and the soil behind the wall is very lengthy, and the geometric size and soil properties remain the same. When the soil behind the wall generates active earth pressure, a slip occurs behind the wall wedge, whose sliding surface is flat and passes through the heel. During the earthquake, the vibration form of the soil at the bottom of the wall is sinusoidal dynamic vibration; seismic acceleration varies with time and depth. This section provides a detailed analysis of the vertical foundation pressure experienced by SM-W1, SM-W2, CR-W W, and GM-W under base excitation conditions. Our study focuses on analysing maximum foundation settlement during base excitation, revealing important insights into the behavior of the walls under seismic loading. The results showed that the pressure decreased with depth below the foundation, indicating a decreasing trend as we moved away from the ground surface.

Furthermore, Fig. 14 indicated that the pressure remained relatively constant from the ground level to the bottom of the wall. This suggests that the foundation settlement stabilizes below a certain depth and does not vary significantly with further depth. The constant pressure distribution is essential to ensure the foundation's stability and integrity and the overall performance of the walls. The results showed that these factors play a significant role in determining the distribution and magnitude of the foundation pressure. As the wall height and depth below the foundation increase, the pressure varies accordingly. Comparing our results with previous researchers allows us to validate and contextualize our findings. By considering the findings of previous studies, such as those by [Damians IP et al., 2016], we can understand the behavior of vertical foundation pressure and its implications for the stability and performance of retaining walls. This comparison helps establish the reliability of our analysis and contributes to the existing body of knowledge in this field. The findings of our study provide valuable insights for designing foundations capable of withstanding seismic loads and preventing foundation damage caused by excessive pressure. Fig. 14 indicates that the upper area of the wall experiences the highest vertical settlement. Similar vertical settlement behavior was observed in GM-W and SM-W2 walls. However, the vertical settlement behavior in the SM-W1 differed from that of the GM-Wand SM-W2.

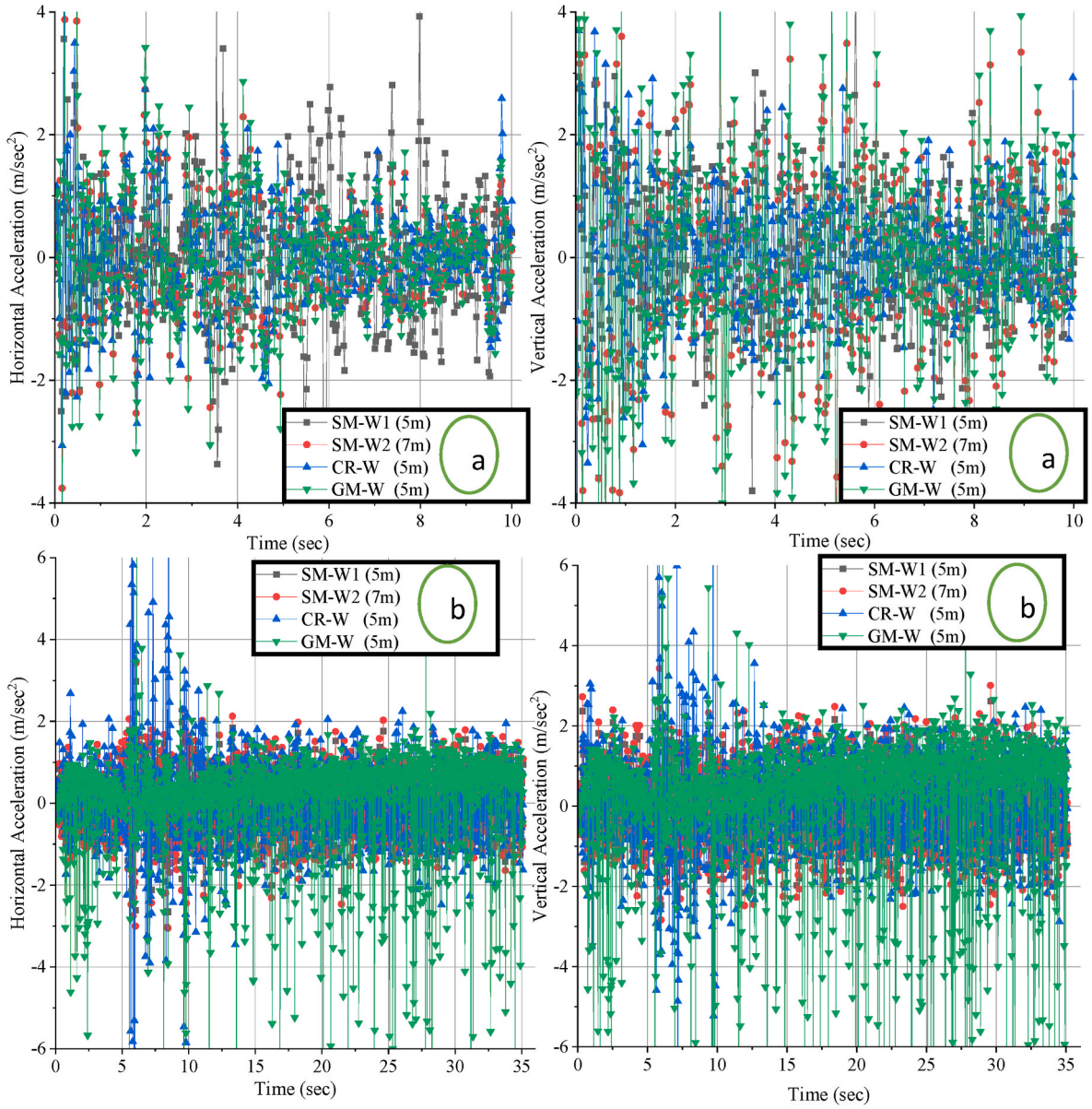

Fig. 13. Acceleration of the wall (a) vertical acceleration of wall (b) horizontal acceleration of wall.

5.7. Displacement of the wall

Through a large number of calculations, it is found that to make the GER wall rotate around a certain point in the wall, the soil behind the wall reaches the plastic limit state, and the overload of the soil surface must be large enough. Otherwise, the limited rotation state around a certain point in the middle will not occur. The analysis of displacement played a crucial role in understanding the structural behavior and response of the walls under seismic loading conditions. When these parameters were examined, valuable insights were obtained regarding the performance and stability of different types of walls. The results of Fig. 15 revealed notable variations in displacement characteristics among the analyzed walls, namely SM-W1, SM-W2, Cr–W, and GM-W. These findings highlight the significance of comprehending and considering these parameters to ensure retaining walls' structural integrity and stability. SM-W1, SM-W2, CR-W, and GM-W demonstrated distinct patterns in their displacement behaviors. Each wall type exhibited specific responses to seismic loading, emphasizing the importance of understanding these characteristics for effective design and analysis. The investigation found that SM-W1 experienced a minimum displacement, GM-W exhibited a maximum displacement, while GM-W recorded a maximum deflection displacement.

To validate the consistency of our results and contribute to the existing body of knowledge, we compared our findings with those of previous researchers who have investigated the behavior of deflection and displacement in retaining walls under seismic loading conditions. For instance, [Tiwari R and Lam N 2021] conducted a study on the dynamic response of retaining walls, including the analysis of deflection and displacement. Their research emphasized the importance of accurate prediction and control of deflection and displacement to ensure the stability and performance of retaining walls under seismic forces. Similarly [Tiwari R and Lam N 2021, Wang L et al., 2015], investigated the behavior of different types of retaining walls under seismic loading, focusing on evaluating deflection and displacement characteristics.

6. Conclusion and policy recommendations

6.1. Conclusion

A comprehensive study investigated the seismic response behavior of

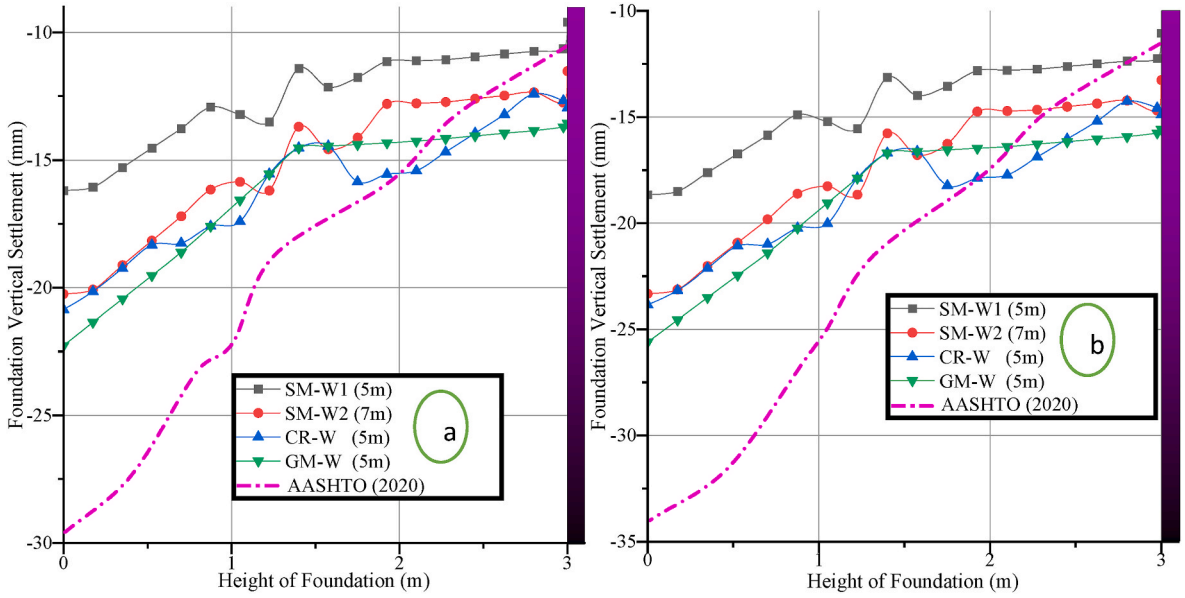

Fig. 14. Vertical settlement of the foundation.

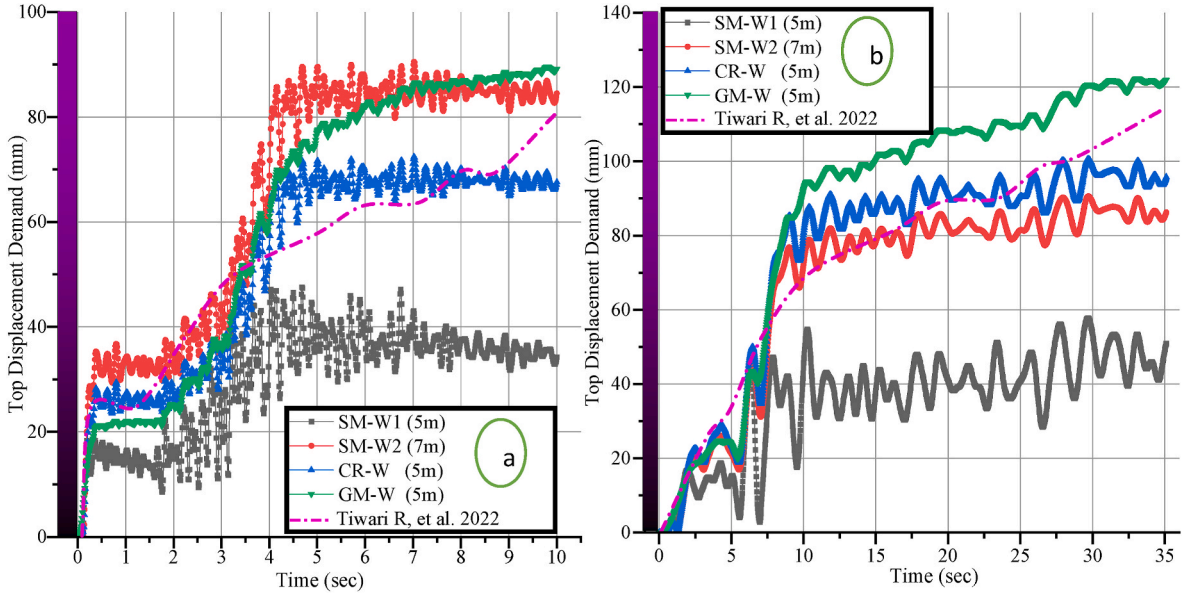

Fig. 15. (a and b). Displacement of the wall.

a GER wall that used granular backfill and reinforcing meshing. Using full-scale finite element analysis, researchers analyzed the seismic response of three models with varying maximum allowed moments of inertia for conventional gravity-type stone masonry and hollow precast concrete GER walls. This research compared the worldwide performance of traditional and prefabricated GER walls under identical environmental and seismic conditions. The following is the conclusion of the analysis.

- The study results indicate a substantial decrease of about 20 % in the sideways force exerted on the valve stem when employing the prefabricated GER wall. Furthermore, a significant reduction in wall displacement, ranging from 30 % to 35 %, has been observed. Regarding seismic response, it can be inferred that prefabricated GER walls exhibit much greater stability compared to reinforced concrete and gravity-type GER walls. The top displacement of GER walls showed a rising tendency as the wall height increased. In contrast, the top displacement of the wall exhibited a positive correlation with its height, reaching its highest point at the topmost section.
- The vertical compaction of the backfill affected the plastic deformation experienced by its surface. The geogrid can significantly decrease the vertical settling of the backfill surfaces. The vertical settling of the backfill surface was much lower in the PC-W reinforced zone compared to the GR-W and CR-W zones. The geogrid enhanced the reinforced GER walls with seismic settlement resistance capacity. The aforementioned study results may be used as reference points for the seismic design and execution of GER walls, including geogrid backfill.
- The deflection angle and mode of displacement of the GER wall impacted the location of resultant force points and the distribution of lateral earth pressure. The earth pressure distribution was nonlinear, and wall displacement was negatively correlated with

pressure. The lowest section exhibited the highest active lateral earth pressure, which negatively correlated with the wall's height. The maximum vertical earth pressure was detected at the backfill's base. The correlation between the resultant force point height and the ultimate state was negative, with a value below 1/2H.

- The deflection level in the upper valve stem of the hollow prefabricated GER wall has dropped by roughly 30 %, and the deflection has reduced by 20–25 %. Prefabricated GER walls have superior seismic performance compared to traditional GER walls, primarily owing to their improved deflection levels. As the wall height grows, the stress distribution reduces. However, the deflection increases, and the highest deflection is seen at the top of reinforced concrete and gravity-type retaining GER walls.
- The walls experienced increased acceleration due to the extended periods of high acceleration values observed in the entire time histories of the ground motions induced by seismic waves. PC-W's acceleration and seismic responses were comparatively lesser than those of CR-W and GM-W in the face of all ground motions.

6.2. Policy recommendation

- The new design is more cost-effective and environmentally friendly, with a 30 % reduction in bottom bar thickness and a 50 % reduction in precast wall volume. Regarding environmental efficiency, the precast concrete GER wall outperformed the conventional (GER) retaining wall; the wall system assembled quickly with little physical effort. The comparative study found that the prefabricated concrete (GER) walls performed better than traditional reinforced concrete GER walls in high seismic areas, including carbon dioxide (CO2) emissions, greenhouse gas (GHG) effects, essential material expenditure, and embodied energy.

Availability of data and materials

All data and models is available per request to the corresponding author.

Ethics approval

(Non-Biological or Non-Medical manuscripts do not need to write this part):

Whether or not the study included human or animal subjects. In all cases, the ethical approval status of the work should be stated in the ethical approval statement.

Funding Statement

This work was supported by Supported by the Science and Technology Research Program of the Institute of Mountain Hazards and Environment, CAS (IMHE-ZDRW-01), and the National Natural Science Foundation of China, China (Grant numbers: 42077275 & 42271086), and the Special project of Basic Research-Key project, Yunnan (Grant numbers: 202301AS070039).

CRediT authorship contribution statement

Muhammad Akbar: Conceptualization, Data curation, Formal analysis, Funding acquisition, Methodology, Validation, Writing – original draft. **Pan Huali:** Supervision, Visualization. **Ou Guoqiang:** Project administration, Resources, Supervision. **Muhammad Usman Arshid:** Formal analysis, Writing – review & editing. **Bilal Ahmad:** Validation, Writing – review & editing. **Tariq Umar:** Writing – review & editing.

Declaration of competing interest

The authors declare that they have no known competing financial interests or personal relationships that could have appeared to influence the work reported in this paper.

Data availability

Data will be made available on request.

Acknowledgment

The authors would like to acknowledge this work to the Institute of Mountain Hazards Environment, Chinese Academy of Sciences, Chengdu, China, for providing us with the platform to conduct this valuable research.

References

[1] L. Wang, G. Chen, S. Chen, Experimental study on seismic response of geogrid reinforced rigid retaining walls with saturated backfill sand, Geotext. Geomembranes 43 (1) (2015) 35–45.
[2] T.M. Allen, R.J. Bathurst, Geosynthetic reinforcement stiffness characterization for MSE wall design, Geosynth. Int. 26 (6) (2019) 592–610.
[3] Aashto, AASHTO LRFD Bridge Design Specifications, ninth ed., American Association of State Highway and Transportation Officials, Washington, DC., USA, 2020.
[4] AFNOR (Association Franc¸aise de Normalisation), Geotechnical Design Retaining Structures Reinforced and Soil Nailing Structures, AFNOR, Paris, 2009, pp. 94–270. NFP.
[5] Geological Survey of Pakistan, GSP, 2022. https://gsp.gov.pk/.
[6] Earthquake Reconstruction & Rehabilitation Authority, ERRA, 2022. http://www.erra.gov.pk/.
[7] R.J. Bathurst, Y. Miyata, T.M. Allen, Deterministic and probabilistic assessment of margins of safety for internal stability of as-built PET strap reinforced soil walls. Geotex Geomembr (Availabe Online), 2020, https://doi.org/10.1016/j.geotexmem.2020.06.001.
[8] J. Bakr, S.M. Ahmad, A finite element performance-based approach to correlate movement of a rigid retaining wall with seismic earth pressure, Soil Dynam. Earthq. Eng. 114 (2018) 460–479.
[9] E. Bourgeois, L. Soyez, A. Le Kouby, Experimental and Numerical study of the behavior of a reinforced-earth wall subjected to a local load, Comput. Geotech. 38 (4) (2011) 515–525.
[10] Z. Cai, R.J. Bathurst, Seismic response analysis of geosynthetic reinforced soil segmental retaining walls by finite element method, Comput. Geotech. 17 (4) (1995) 523–546.
[11] A. Ardah, M. Abu-Farsakh, G. Voyiadjis, Numerical evaluation of the performance of a geosynthetic reinforced soil-integrated bridge system (GRS-IBS) under different loading conditions, Geotext. Geomembranes 45 (6) (2017) 558–569.
[12] Q.-G. Yang, H. Liu, T.-Y. Zhou, L.-B. Xiong, Post-construction performance of a two-tiered geogrid reinforced soil wall backfilled with soil-rock mixture, Geotext. Geomembranes 42 (2) (2014) 91–97.
[13] I.P. Damians, R.J. Bathurst, A. Josa, A. Lloret, Numerical analysis of an instrumented steel reinforced soil wall, ASCE Int J Geomech 15 (1) (2015) 04014037.
[14] I.P. Damians, R.J. Bathurst, A. Josa, A. Lloret, Vertical facing panel-joint gap analysis for steel-reinforced soil walls, ASCE Int J Geomech 16 (4) (2016) 04015103.
[15] T. Cakir, Evaluation of the effect of earthquake frequency content on seismic behavior of cantilever retaining wall including soil–structure interaction, Soil Dynam. Earthq. Eng. 45 (2013) 96–111.
[16] H. Fathipour, A.S. Siahmazgi, M. Payan, R.J. Chenari, Evaluation of the lateral earth pressure in unsaturated soils with finite element limit analysis using second-order cone programming, Comput. Geotech. 125 (2020) 103587.
[17] H. Fathipour, M. Payan, R.J. Chenari, Limit analysis of lateral earth pressure on geosynthetic-reinforced retaining structures using finite element and second-order cone programming, Comput. Geotech. 134 (2021) 104119.
[18] S. Aroni Hesari, S. Javankhoshdel, M. Payan, R. Jamshidi Chenari, Pseudo-static internal stability analysis of geosynthetic-reinforced earth slopes using horizontal slices method, Geomechanics Geoengin. 17 (5) (2022) 1417–1442.
[19] S.M. Mirmoazen, S.H. Lajevardi, S.M. Mirhosseini, M. Payan, R. Jamshidi Chenari, Limit analysis of lateral earth pressure on geosynthetic-reinforced retaining structures subjected to strip footing loading using finite element and second-order cone programming, Iranian Journal of Science and Technology, Transactions of Civil Engineering 46 (4) (2022) 3181–3192.
[20] Sanjay Nimbalkar, Deepankar Choudhury, Sliding stability and seismic design of retaining wall by pseudo-dynamic method for passive case, Soil Dynam. Earthq. Eng. 27 (6) (2007) 497–505, https://doi.org/10.1016/j.soildyn.2006.11.006.
[21] D.G. Anderson, Seismic Analysis and Design of Retaining Walls, Buried Structures, Slopes, and Embankments, vol. 611, Transportation Research Board, 2008.

[22] Emin Hokelekli, Betul Nihan Yilmaz, Effect of cohesive contact of backfill with arch and spandrel walls of a historical masonry arch bridge on seismic response 63 (3) (2019) 926–937.
[23] J. Lee, G.L. Fenves, Plastic-damage model for cyclic loading of concrete structures, J. Eng. Mech. 124 (8) (1998) 892–900.
[24] S. Bahmani Tajani, H. Fathipour, M. Payan, R. Jamshidi Chenari, K. Senetakis, Temperature-dependent lateral earth pressures in partially saturated backfills, European Journal of Environmental and Civil Engineering 27 (10) (2023) 3064–3090.
[25] M. Akbar, H. Pan, G. Ou, G. Nikitas, B. Ahmad, Seismic response compression of various MSE walls based on 3D modeling, Buildings 13 (11) (2023) 2773, https://doi.org/10.3390/buildings13112773.
[26] H. Munoz, F. Tatsuoka, D. Hirakawa, H. Nishikiori, R. Soma, M. Tateyama, K. Watanabe, Dynamic stability of geosynthetic- reinforced soil integral bridge, Geosynth. Int. 19 (1) (2012) 11–38.
[27] A. Osouli, S. Zamiran, The effect of backfill cohesion on seismic response of cantilever retaining walls using fully dynamic analysis, Comput. Geotech. 89 (2017) 143–152.
[28] A. Athanasopoulos Zekkos, V.S. Vlachakis, A.-G. Athanasopoulos, Phasing issues in the seismic response of yielding, gravity-type earth retaining walls – overview and results from a FEM study, Soil Dynam. Earthq. Eng. 55 (2013) 59–70.
[29] M. Yazdandoust, Investigation on the seismic performance of steel-strip reinforced-soil retaining walls using shaking table test, Soil Dynam. Earthq. Eng. 97 (2017) 216–232.
[30] T.M. Allen, R.J. Bathurst, An improved simplified method for prediction of loads in reinforced soil walls, ASCE J Geotechn Geoenviron Eng 141 (11) (2015) 04015049.
[31] Fhwa, Design of mechanically stabilized earth walls and reinforced slopes, in: R. R. Berg, B.R. Christopher, N.C. Samtani (Eds.), No. FHWA-NHI-10-024 Vol I and NHI-10-025 Vol II, Federal Highway Administration, Washington, DC., USA, 2009.
[32] C. Yoo, S.B. Kim, Performance of a two-tier geosynthetic reinforced segmental retaining wall under a surcharge load: fullscale load test and 3D finite element analysis, Geotext. Geomembranes 26 (6) (2008) 460–472.
[33] H. Liu, Long-term lateral displacement of geosynthetic-reinforced soil segmental retaining walls, Geotext. Geomembranes 32 (2012) 18–27.
[34] Y. Yu, R.J. Bathurst, T.M. Allen, R. Nelson, Physical and numerical modelling of a geogrid reinforced incremental concrete panel retaining wall, Can. Geotech. J. 53 (12) (2016) 1883–1901.
[35] C. Choufani, P. Wu, G. Gagnon, M. Macintosh, A precast faced mechanical stabilized earth solution for a 20-metre-high mining crusher wall with various technical and site challenges, in: Proceedings of 2011 Pan-Am Canadian Geotechnical Conference (CD-ROM), Canadian Geotechnical Society, Richmond, BC, Canada, 2011, p. 625.
[36] A.K. Tiwary, et al., Performance comparison and critical finite element based experimental analysis of various forms of reinforcement retaining structural system. https://doi.org/10.1155/2022/4434679, 2022.
[37] J. Vlcek, Internal stability analyses of geosynthetic reinforced retaining walls, Procedia Eng. 91 (2014) 346–351.
[38] Abaqus/explicit User's manual, version 6.13, Dassault Syste'mes Simulia Corporation, Rhode Island, Providence, 2013. USA).
[39] W. Zhang, J.F. Chen, Y. Yu, Influence of toe restraint conditions on performance of geosynthetic-reinforced soil retaining walls using centrifuge model tests, Geotext. Geomembranes 47 (5) (2019) 653–661.
[40] M. Ahmadabadi, A. Ghanbari, New procedure for active earth pressure calculation in retaining walls with reinforced cohesive-frictional backfill, Geotext. Geomembranes 27 (6) (2009) 456–463.
[41] I.E. Zevgolis, A finite element investigation on displacements of reinforced soil walls under the effect of typical traffic loads, Transp Infrastruct Geotechnol 5 (3) (2018) 231–249.
[42] C.S. Vieira, M.d.L. Lopes, L.M. Caldeira, Earth pressure coefficients for design of geosynthetic reinforced soil structures, Geotext. Geomembranes 29 (5) (2011) 491–501.
[43] R. Tiwari, N. Lam, Modelling of seismic actions in earth retaining walls and comparison with shaker table experiment, Soil Dynam. Earthq. Eng. 150 (2021) 106939.
[44] M.M. Lima, et al., The effects of CFRP orientation on the strengthening of reinforced concrete structures, Struct. Des. Tall Special Build. 25 (15) (2016) 759–784.
[45] J. Lubliner, J. Oliver, S. Oller, E. Oñate, et al., A plastic-damage model for concrete, Int. J. Solid Struct 1989 (1989) 299–326, https://doi.org/10.1016/0020-7683(89)90050-4.
[46] J. Lee, G.L. Fenves, Plastic-damage model for cyclic loading of concrete structures, J. Eng. Mech. 124 (8) (1998) 892–900.
[47] D.J. Carreira, K.H. Chu, Stress-strain relationship for plain concrete in compression, J Proc 82 (6) (1985) 797–804.